Angular dependence of magnetoresistance in strongly anisotropic quasi-two-dimensional metals: Influence of Landau-level shape

P. D. Grigoriev*
L. D. Landau Institute for Theoretical Physics, 142432 Chernogolovka, Russia

T. I. Mogilyuk
National Research Centre "Kurchatov Institute", Moscow, Russia
(Received 19 September 2013; published 22 September 2014)

We present the quantum-mechanical calculation of the angular dependence of interlayer conductivity $\sigma_{zz}(\theta)$ in a tilted magnetic field in quasi-two-dimensional (quasi-2D) layered metals. Our calculation is applicable for arbitrary density of electron states and shows that the shape of Landau levels (LLs) is important for this angular dependence. We derive simple analytical formulas for $\sigma_{zz}(\theta)$ in the particular cases of Gaussian and dome-shaped LLs. Since in strongly anisotropic quasi-two-dimensional metals in a high magnetic field the LL shape is closer to dome-like or Gaussian, this analytical formula replaces the traditionally used one, derived for Lorentzian LL shape. The amplitude of angular magnetoresistance oscillations (AMRO) is considerably stronger for the dome-like or Gaussian than for the traditionally used Lorentzian LL shape. The ratio $\sigma_{zz}(\theta=0)/\sigma_{zz}(\theta\to\pm 90^\circ)$ is also several times smaller for the Lorentzian LL shape at the same LL width. The field dependence of $\sigma_{zz}(\theta\to\pm 90^\circ)$ provides useful information about the electron mean free time. AMRO and Zeeman energy splitting lead to a spin current. For typical organic metals and for a medium magnetic field of 10 T this spin current is only a few percent of the charge current. However, the spin current may almost reach the charge current for special tilt angles of the magnetic field. The spin current has strong angular oscillations, which are phase-shifted as compared to the usual AMRO.

DOI: 10.1103/PhysRevB.90.115138 PACS number(s): 72.15.Gd, 73.43.Qt, 74.70.Kn, 74.72.−h

I. INTRODUCTION

Angular magnetoresistance oscillations (AMRO) are a prominent feature of strongly anisotropic layered conductors, which give important information about their electronic properties (see, e.g., [1–3] for reviews). AMRO are actively used to investigate various layered compounds, including organic metals [1–7], high-temperature cuprate superconductors [8–12], heterostructures [13], etc.

AMRO were first observed [14] in 1988 in the quasi-two-dimensional (quasi-2D) strongly anisotropic organic metal β-(BEDT-TTF)$_2$IBr$_2$. The first explanation of AMRO appeared the next year [15] and used the geometrical arguments for the Fermi surface of the corrugated-cylinder shape, which corresponds to strongly anisotropic electron dispersion,

$$\epsilon_{3D}(\mathbf{k}) \approx \epsilon_{2D}(k_x,k_y) - 2t_z\cos(k_z d), \tag{1}$$

where $\hbar k_z$ is the out-of-plane electron momentum, $\hbar$ is Planck's constant, d is the interlayer spacing, and the interlayer transfer integral t_z is much less than the Fermi energy E_F. For the quadratic and isotropic in-plane electron dispersion $\epsilon_{2D}(k_x,k_y) = \hbar^2(k_x^2+k_y^2)/2m^*$, Yamaji obtained [15] that the minima of interlayer conductivity $\sigma_{zz}(\theta)$ correspond to the zeros of $J_0(\kappa)$, where J_0 is the Bessel function of the zeroth order, $\kappa \equiv k_F d\tan\theta$, k_F is the in-plane Fermi momentum, and θ is the angle between the applied magnetic field $\boldsymbol{B}$ and the normal to the conducting planes. The direct calculation of interlayer conductivity, using the electron dispersion in Eq. (1) and the Boltzmann transport equation in the τ approximation, gives [16]

$$\sigma_{zz} = \sigma_{zz}^0 \left\{ [J_0(\kappa)]^2 + 2\sum_{\nu=1}^{\infty} \frac{[J_\nu(\kappa)]^2}{1+(\nu\omega_c\tau)} \right\}, \tag{2}$$

where the cyclotron frequency $\omega_c \equiv eB_z/m^*c \equiv \omega_{c0}\cos\theta$, τ is the mean free time, and the interlayer conductivity without magnetic field

$$\sigma_{zz}^0 = e^2\rho_F\langle v_z^2\rangle\tau = 2e^2t_z^2m^*\tau d/\pi\hbar^4, \tag{3}$$

where $\rho_F = m^*/\pi\hbar^2 d$ is the 3D density of states (DoS) at the Fermi level in the absence of magnetic field per two spin components, and the mean squared interlayer electron velocity $\langle v_z^2\rangle = 2t_z^2d^2/\hbar^2$. Here e is the electron charge, m^* is the effective electron mass, B_z is the component of the magnetic field perpendicular to conducting layers, and c is the light velocity. Equation (2) agrees with the result of Yamaji at $\omega_c\tau\to\infty$. A microscopic calculation [17] of quasi-2D AMRO also gives Eq. (2) when the number of filled Landau levels (LLs) $n_{LL}^F \gg 1$.

Equation (2) describes the dependence of conductivity on the polar tilt angle θ of the magnetic field only, because it assumes an isotropic in-layer dispersion $\epsilon_{2D}(k_x,k_y)$. Its generalization for the anisotropic in-plane dispersion also within the τ approximation was considered analytically in Refs. [18–20]. and numerically in Refs. [8–11], which gives the azimuthal-angle dependence of magnetoresistance (MR).

The calculations of AMRO in Refs. [15–21] assume a well-defined 3D electron dispersion (1), i.e., that the LL separation $\hbar\omega_c$ and broadening $\Gamma = \hbar/2\tau$ are much less than t_z. In these works the electron mean free time is taken to be constant and the same as without magnetic field: $\tau=\tau_0$. The inverse "weakly incoherent" limit $t_z \ll \Gamma_0$ with

*Corresponding author: grigorev@itp.ac.ru

the momentum-conserving "coherent" interlayer hopping was studied in Ref. [22], where the interlayer conductivity was calculated as a tunneling conductivity between two adjacent conducting layers, again resulting in Eq. (2). The calculations in Refs. [17,22] also assume that the electron self-energy $\mathrm{Im}\,\Sigma = \Gamma_0 = \hbar/2\tau_0$ is independent of energy and magnetic field. This assumption, being almost equivalent to the τ approximation, is incorrect in 2D or strongly anisotropic quasi-2D layered compounds with $t_z, \Gamma_0 \lesssim \hbar\omega_c$, i.e., in the presence of strong magnetic quantum oscillations (MQO) [23–33]. Even if MQO are suppressed by temperature, which smears the Fermi distribution function [34–36], these MQO produce the monotonic growth [29–33,37] of the longitudinal interlayer magnetoresistance $R_{zz}(B_z) = 1/\sigma_{zz}$ and of the LL broadening $\Gamma = \Gamma(B_z)$, which changes the angular dependence $R_{zz}(\theta)$ [29].

In Ref. [29] a semi-phenomenological amendment to Eq. (2) in the limit $t_z \ll \Gamma_0$ was proposed (see Eq. (36) of Ref. [29]). This amendment includes the renormalization of the prefactor,

$$\sigma_{zz}^0 \to \sigma_{zz}^0(B_z) \approx \sigma_{zz}^0[1 + (2\omega_c\tau_0)^2]^{-1/4}, \tag{4}$$

and the similar renormalization of the effective mean scattering time in Eq. (2):

$$\tau \to \tau(B_z) \approx \tau_0[1 + (2\omega_c\tau_0)^2]^{-1/4}. \tag{5}$$

However, the calculation in Ref. [29] has several drawbacks. First, the derivation of Eq. (2) and all previous calculations of AMRO disregard the additional "quantum" term, coming from MQO and first obtained in Refs. [25–27] for magnetic field perpendicular to the conducting layers. For tilted magnetic field this "quantum" term is given by the second term in the curly brackets in Eq. (6) below or in Eq. (29) of Ref. [29]. Second, and more importantly, Eq. (2) is derived assuming the Lorentzian LL shape. In strongly anisotropic quasi-2D layered metals with $t_z \ll \hbar\omega_c$ and in high magnetic field; i.e., at $\omega_c\tau \gg 1$, the actual LL shape is not Lorentzian but rather Gaussian [33], similar to that in 2D conductors [24,38–46].

The question about the influence of the LL shape on the angular dependence of magnetoresistance has not been addressed so far, and all previous AMRO calculations were performed for the Lorentzian LL shape. The present report is mostly aimed to fill this gap of knowledge. Below we show by direct calculation that AMRO appreciably depend on the LL shape, i.e., on the DoS profile of each LL. This is important for analyzing the experimental data on AMRO and for extracting the $\omega_c\tau$ value from these data. We also derive the analytical formula for AMRO in the case of Gaussian LL shape [see Eq. (34)], which replaces Eq. (2) in the limit $t_z \ll \hbar\omega_c$. In addition, we show [see Eq. (17)] that the usually neglected "quantum term" does not considerably affect the angular dependence of the monotonic part of MR, contributing only to MQO.

The present theoretical study is also motivated by the appreciable discrepancy in AMRO amplitude between Eq. (2) and the experiments in various organic metals. For example, consider the AMRO data reported in Fig. 1 of Ref. [47]. Taking the reported value $\tau \approx 5$ ps, and substituting the effective mass $m^* = 1.3m_e$ for this compound at pressure ~ 6 kbar, we obtain $\omega_c\tau \approx 0.34$ for the dirty sample in Ref. [47] at $B = 0.5$ T.

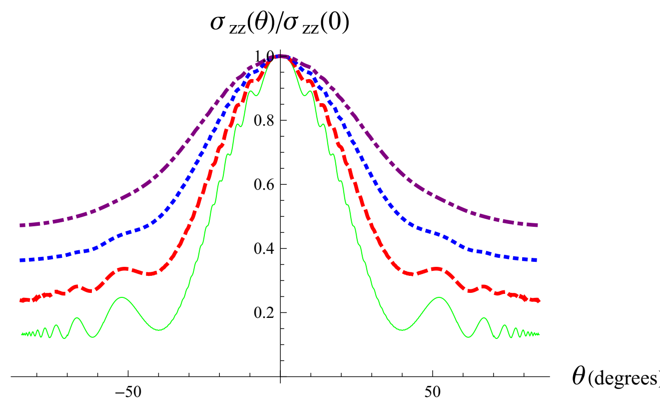

FIG. 1. (Color online) The angular dependence of normalized interlayer conductivity, calculated using Eqs. (18) and (19) for the Lorentzian LL shape with four different values of $\omega_c\tau_0 = 10$ (thin solid green curve), 10/3 (dashed red curve), 5/3 (dotted blue curve), and 1 (dash-dotted purple curve). The other parameters are $k_F d = 3$, $\mu = 605$ K, $T = 3$ K, and $B_0 \approx 11.6$ T, which for cyclotron mass $m^* = m_e$ and for $\theta = 0$ corresponds to $\hbar\omega_c = 10$ K.

According to Eq. (2) at $\omega_c\tau \approx 0.34$ AMRO should not be visible at all. Even at $\omega_c\tau = 1$ AMRO are not visible (see Fig. 1 of Ref. [22]). This prediction contradicts the experimental data in Fig. 1 of Ref. [47], where at least first two AMRO maxima are clearly observed at $B = 0.5$ T. Possibly, this discrepancy can be attributed to the different $\omega_c\tau$ values, which enter the formulas for the amplitudes of MQO and of AMRO. However, a theoretical study of AMRO for the non-Lorentzian LL shape is need for better understanding this issue. The clearly non-Lorentzian LL shape was demonstrated in the quasi-2D organic metal α-(BEDT-TTF)$_2$KHg(SCN)$_4$ by analyzing the damping of various harmonics of MQO [33].

In Sec. II we write down the formulas for AMRO which are valid for arbitrary LL shape. In Sec. III we obtain explicit results for the Lorentzian, Gaussian, and dome-like LL shapes. In Sec. IV we analyze the general angular dependence of magnetoresistance and the ratio $\sigma_{zz}(\theta \to \pm 90^\circ)/\sigma_{zz}(\theta = 0)$ for various LL shapes. We will show that the field dependence of $\sigma_{zz}(\theta \to \pm 90^\circ)$ provides useful information about the τ_0 value, which may considerably differ from the τ value obtained from AMRO amplitude or from Dingle temperature. In Sec. V we study the spin current, which is produced by AMRO and Zeeman splitting. Section VI gives concluding remarks.

II. CALCULATIONS FOR ARBITRARY LANDAU-LEVEL SHAPE

To calculate the interlayer conductivity σ_{zz}, we apply the two-layer model as in Refs. [22,29]. It includes two adjacent conducting layers with short-range impurities and with a coherent interlayer electron hopping, which conserves the in-plane electron momentum (see Eqs. (8)–(11) of Ref. [29]). This model is applicable when the interlayer transfer integral t_z is less than the LL broadening [32]. The interlayer conductivity can be calculated using the Kubo formula, which for one spin component gives Eq. (29) of Ref. [29]. It contains an extra "quantum term" as compared to Eq. (50) of Ref. [22], and after the addition of the summation over spin index $s = \pm 1$, it becomes

$$\sigma_{zz} = \frac{e^2 t_z^2 d}{\pi\hbar} \sum_{s=\pm 1} \int d\varepsilon [-n_F'(\varepsilon)] \times \int d^2\boldsymbol{r} \{ |\langle G(\boldsymbol{r},\varepsilon_s)\rangle|^2 \cos(qy) - \mathrm{Re}[\langle G(\boldsymbol{r},\varepsilon_s)\rangle \langle G(-\boldsymbol{r},\varepsilon_s)\rangle e^{iqy}]\}. \tag{6}$$

Here $n_F'(\varepsilon) = -1/\{4T \cosh^2[(\varepsilon-\mu)/2T]\}$ is the derivative of the Fermi distribution function, μ is the chemical potential, $\boldsymbol{r} \equiv \{x,y\}$, $\varepsilon_s = \varepsilon + s\mu_B B$, μ_B is the Bohr magneton, $q \equiv eBd \sin\theta/\hbar c$, and $\langle G(\boldsymbol{r},\varepsilon)\rangle = \langle G(\boldsymbol{r}_1,\boldsymbol{r}_1+\boldsymbol{r},\varepsilon)\rangle$ is the retarded electron Green's function as function of coordinate and energy, averaged over impurity positions. The impurity averaging of each Green's function in Eq. (6) is performed separately, because the vertex corrections have the next order of smallness in the parameter t_z and because the impurities are short-range. For short-range impurities in the noncrossing approximation the averaged electron Green's function is given by [24,29]

$$G(\boldsymbol{r}_1,\boldsymbol{r}_2,\varepsilon) = \sum_{n,k_y} \Psi^*_{n,k_y}(r_2)\Psi_{n,k_y}(r_1) G(\varepsilon,n), \tag{7}$$

where n is the LL number,

$$G(\varepsilon,n) = \frac{1}{\varepsilon - \epsilon_{2D}(n) - \Sigma(\varepsilon)}, \tag{8}$$

and the 2D electron dispersion in a magnetic field, $\epsilon_{2D}(n) \equiv \epsilon_n = \hbar\omega_c(n+1/2)$. In the noncrossing approximation the electron self-energy part $\Sigma(\varepsilon)$ depends only on energy ε (see Appendix of Ref. [29]), being a periodic function with the period $\hbar\omega_c$, and Eq. (7) contains the bare electron wave functions

$$\Psi_{n,k_y}(r) = \Psi_n\left(x - l_H^2 k_y\right)\exp(ik_y y), \tag{9}$$

where

$$\Psi_n(x) = \frac{\exp\left(-x^2/2l_H^2\right) H_n(x/l_H)}{\left(\pi l_H^2\right)^{1/4} 2^{n/2}\sqrt{n!}}, \tag{10}$$

$H_n(x/l_H)$ is the Hermite polynomial, and $l_H = \sqrt{\hbar c/eB_z}$ is the magnetic length.

In strong magnetic field $\hbar\omega_c \gg \Gamma_0$ the electron Green's function $G(\varepsilon,n)$ can be calculated by restricting to only one LL at $\varepsilon \approx \varepsilon_{2D}(n)$, which in the noncrossing approximation gives a dome-like rather than Lorentzian LL shape [24]. The inclusion of diagrams with the intersection of impurity lines adds the exponential tails in the electron DoS $\rho(\varepsilon) = -\mathrm{Im}\, G(\varepsilon,n)/\pi$ for each LL [38]. Since MR depends on the LL shape, we first calculate Eq. (6) without restriction to any particular form of the electron Green's function, and then compare the results for various LL shapes.

Now we substitute the electron Green's function from Eq. (7) to Eq. (6). The first term in curly brackets, coinciding with Eq. (50) of Ref. [22] and responsible for the so-called "classical" $G_R G_A$ part of conductivity σ_{zz}, is rewritten as (see Appendix A)

$$Cl \equiv \int d^2 r |G(r,\varepsilon)|^2 \cos(qy) = g_{LL} \sum_{n,p\in Z} [\mathrm{Re}G(\varepsilon,n)\mathrm{Re}G(\varepsilon,n+p) + \mathrm{Im}G(\varepsilon,n)\mathrm{Im}G(\varepsilon,n+p)]\, Z(n,p), \tag{11}$$

where the LL degeneracy per unit area $g_{LL} = 1/2\pi l_H^2 = eB_z/2\pi\hbar c$,

$$Z(n,p) = \exp\left(-\frac{(ql_H)^2}{2}\right)\left(\frac{(ql_H)^2}{2}\right)^p \times \left[L_n^p\left(\frac{(ql_H)^2}{2}\right)\right]^2 \left(\frac{n!}{(n+p)!}\right), \tag{12}$$

and $L_n^p(x)$ is the Laguerre polynomial. The second term in curly brackets in Eq. (6), which is absent in Refs. [16,22] and responsible for the so-called "quantum" part of conductivity σ_{zz}, is rewritten as (see Appendix B)

$$Q \equiv \mathrm{Re}\left[\int d^2 r\, \langle G(\boldsymbol{r},\varepsilon)\rangle^2 \exp(iqy)\right] = g_{LL} \sum_{n,p\in Z} [\mathrm{Re}G(\varepsilon,n)\mathrm{Re}G(\varepsilon,n+p) - \mathrm{Im}G(\varepsilon,n)\mathrm{Im}G(\varepsilon,n+p)]\, Z(n,p). \tag{13}$$

When many Landau levels (LL) are filled, i.e. at $n \sim n_{LL}^F \equiv \lceil \mu/\hbar\omega_c \rceil \gg 1$, one can use the asymptotics of Laguerre polynomials,

$$L_n^\alpha(z) \approx \frac{\Gamma(\alpha+n+1)}{n!}\left[\left(n+\frac{\alpha+1}{2}\right)z\right]^{-\frac{\alpha}{2}} \times \exp\left(\frac{z}{2}\right) J_\alpha\left(2\sqrt{\left(n+\frac{\alpha+1}{2}\right)z}\right), \tag{14}$$

which gives at $0 \leqslant p \ll n$

$$Z(n,p) \approx J_p^2(\sqrt{2n+1}\, ql_H). \tag{15}$$

Equation (15) can be further simplified using $\sqrt{2n_{LL}^F+1}\, ql_H \approx k_F d\tan\theta$ and that $Z(n,p)$ has a weak dependence on n:

$$Z(n,p) \approx Z(n_{LL}^F,p) \approx J_p^2(k_F d\tan\theta) \equiv J_p^2(\kappa). \tag{16}$$

Now we can answer the question how the additional "quantum" term affects AMRO of the monotonic part of interlayer conductivity. Substituting Eqs. (16) and (8) into Eq. (13) and applying the Poisson summation formula for the summation over n, we obtain for the zeroth harmonic of Q

$$\bar{Q} \approx \sum_{p\in Z} \frac{J_p^2(k_F d\tan\theta)}{(\hbar\omega_c)^2} \times \int_{-\infty}^{\infty} \frac{dn[(n-u)(n+p-u)-v^2]}{[(n-u)^2+v^2][(n+p-u)^2+v^2]} = 0, \tag{17}$$

where $u \equiv [\varepsilon - \mathrm{Re}\Sigma(\varepsilon)]/\hbar\omega_c - 1/2$ and $v \equiv \mathrm{Im}\,\Sigma(\varepsilon)/\hbar\omega_c$. The integral over n in Eq. (17) is zero for each p, because the residues in the poles at $n = u + iv$ and $n = u - p + iv$ cancel each other for each $p \neq 0$, while at $p = 0$ the residue is zero, which can be checked by a direct calculation. Hence, when many LL are filled so that Eq. (16) is valid, $\bar{Q} \approx 0$. One can show, taking the dependence $Z(n,p)$ in Eq. (12) into account, that $\bar{Q}$ is smaller than the classical part Cl by a factor $\sim p\, dZ(n,p)/dn \sim p/n \ll 1$. This statement does not depend on the LL shape, because Eq. (17) is valid for arbitrary $\Sigma(\varepsilon)$.

Interlayer conductivity

$$\sigma_{zz}(T) = \frac{1}{2}\sum_{s=\pm 1}\int d\varepsilon[-n_F'(\varepsilon)]\sigma_{zz}(\varepsilon + s\mu_B B), \quad (18)$$

where $\sigma_{zz}(\varepsilon) = (Cl - Q)\, 2e^2 t_z^2 d/\pi\hbar$, which gives

$$\frac{\sigma_{zz}(\varepsilon)}{\sigma_{zz}^0} = \frac{2\Gamma_0\hbar\omega_c}{\pi}\sum_{n,p\in Z} Z(n,p)\mathrm{Im}G(\varepsilon,n)\mathrm{Im}G(\varepsilon,n+p), \quad (19)$$

and the interlayer conductivity in the absence of magnetic field is given by Eq. (3): $\sigma_{zz}^0 = 2e^2 g_{LL} t_z^2 d/\hbar^2\omega_c\Gamma_0 = 2e^2\tau_0 m^* t_z^2 d/\pi\hbar^4$. Equation (19) is valid for arbitrary electron Green's function $G(\varepsilon,n)$ and will be used in Sec. III to analyze AMRO for various LL shapes.

At $\hbar\omega_c \ll T \ll \mu$, i.e., when the MQO are damped by temperature, the integration over energy in Eq. (18) is equivalent to the averaging over the period of MQO:

$$\sigma_{zz}(T) = \frac{1}{2}\sum_{s=\pm 1}\int d\varepsilon[-n_F'(\varepsilon)]\sigma_{zz}(\varepsilon + s\mu_B B) \approx \bar{\sigma}_{zz}, \quad (20)$$

where

$$\bar{\sigma}_{zz} = \int_{\hbar\omega_c n_F}^{\hbar\omega_c(n_F+1)} \sigma_{zz}(\varepsilon)\frac{d\varepsilon}{\hbar\omega_c}. \quad (21)$$

Substituting Eq. (16) into Eqs. (19)–(21), we obtain

$$\begin{aligned}\frac{\bar{\sigma}_{zz}}{\sigma_{zz}^0} &= \frac{2\Gamma_0}{\pi}\int_{\hbar\omega_c n_F}^{\hbar\omega_c(n_F+1)} d\varepsilon \sum_{n,p\in Z} J_p^2(\kappa) \\ &\quad\times \mathrm{Im}G(\varepsilon,n)\mathrm{Im}G(\varepsilon,n+p) \\ &= \frac{2\Gamma_0}{\pi}\int_{-\infty}^{\infty} d\varepsilon \sum_{p\in Z} J_p^2(\kappa)\,\mathrm{Im}G(\varepsilon,n)\mathrm{Im}G(\varepsilon,n+p).\end{aligned} \quad (22)$$

III. AMRO FOR VARIOUS LL SHAPES

In a strong magnetic field, $\hbar\omega_c \gg \Gamma$, the details of AMRO may essentially depend on the LL shape, determined by the Green's function $G(\varepsilon,n)$ or, equivalently, by the function $\Sigma(\varepsilon)$. The commonly used formula for AMRO, given by Eq. (2), is derived for the Lorentzian LL shape. However, in 2D and strongly anisotropic quasi-2D layered compounds in a strong magnetic field, when $\omega_c\tau \gg 1$, the LL shape is not Lorentzian [24,33,38–46]. Below, using Eqs. (18) and (19) valid for arbitrary LL shape, we calculate and compare AMRO for three microscopically derived and generally used LL shapes.

A. AMRO for the Lorentzian LL shape

In 3D metals the impurity scattering leads to the Lorentzian broadening of electron levels [35,36]. Therefore, in the limit $4t_z \gg \Gamma_0, \hbar\omega_c$ the broadening of electron levels is also close to Lorentzian. Moreover, in the limit $\Gamma_0 \gg \hbar\omega_c$ at arbitrary t_z the quantum oscillations of the electron self-energy $\Sigma(\varepsilon)$ in SCBA are predicted to be much weaker than its average value [26,37], which also corresponds to the Lorentzian shape of LLs.

For the Lorentzian LL shape in Eq. (8) the electron self-energy $\Sigma(\varepsilon) = i\Gamma = i\hbar/2\tau$ is independent of ε, and the DoS of each LL is given by

$$D(E) = \frac{|\mathrm{Im}G(E)|}{\pi} = \frac{\Gamma/\pi}{E^2 + \Gamma^2}, \quad (23)$$

where $E = \varepsilon - \epsilon_{2D}(n) - \mathrm{Re}\,\Sigma(\varepsilon)$. This approximation/assumption has been used in Refs. [22,29], and for the monotonic part $\bar{\sigma}_{zz}^L$ of interlayer conductivity one confirms Eq. (2) with $\tau = \hbar/2\Gamma$. The monotonic field dependence of electron self-energy $\mathrm{Im}\,\Sigma(\varepsilon) = \Gamma(B_z)$, included in Ref. [29], only leads to the renormalization of σ_{zz}^0 and τ according to Eqs. (4) and (5).

The derivation of Eq. (2) for the Lorentzian LL shape using Eq. (22) is much simpler than in Ref. [22]. Substituting Eq. (23) into Eq. (22) and taking the integral

$$\begin{aligned}&\int_{-\infty}^{\infty} dE\,|\mathrm{Im}G(E)|\,|\mathrm{Im}G(E+p\hbar\omega_c)| \\ &= \int_{-\infty}^{\infty} dE\frac{\Gamma}{E^2+\Gamma^2}\frac{\Gamma}{(E+p\hbar\omega_c)^2+\Gamma^2} \\ &= \frac{\pi}{2\Gamma}\frac{1}{1+(p\hbar\omega_c/2\Gamma)^2},\end{aligned}$$

we obtain

$$\frac{\bar{\sigma}_{zz}}{\sigma_{zz}^0} = \frac{\Gamma_0}{\Gamma}\sum_{p\in Z}\frac{J_p^2(\kappa)}{1+(p\hbar\omega_c/2\Gamma)^2}, \quad (24)$$

which coincides with Eq. (2).

In Fig. 1 we plot the angular dependence of normalized interlayer conductivity, calculated using Eqs. (18) and (19) for the Lorentzian LL shape with four different values of $\Gamma_0 = \hbar/2\tau_0$: $\Gamma_0 = 0.5$ K (thin solid green curve), $\Gamma_0 = 1.5$ K (dashed red curve), $\Gamma_0 = 3.0$ K (dotted blue curve), and $\Gamma_0 = 5.0$ K (dash-dotted purple curve). The other parameters are $k_F d = 3$, $\mu = 605$ K, $T = 3$ K, and $B_0 \approx 11.6$ T, which for cyclotron mass $m^* = m_e$ and for $\theta = 0$ corresponds to $\hbar\omega_c = 10$ K. Hence, the four curves in Fig. 1 correspond to four values of $\omega_c\tau_0 = 10$, 10/3, 5/3, and 1, when the magnetic field is perpendicular to conducting layers. In a tilted field the perpendicular-to-layers component of the magnetic field B_z decreases: $B_z = B_0\cos\theta$, and the values of $\omega_c\tau_0$ also decrease $\propto \cos\theta$. In the Lorentzian Green's function we use the renormalized $\Gamma(B_z) = \Gamma_0[1 + (2\omega_c\tau_0)^2]^{1/4}$, corresponding to Eq. (5) and Ref. [29]. Then the renormalization of $\sigma_{zz}(B_z)$, given by Eq. (4), appears automatically from the calculation. Except for the fast quantum oscillations, the curves in Fig. 1 coincide with the AMRO curves calculated using Eqs. (2), (4), and (5) and shown in Ref. [29].

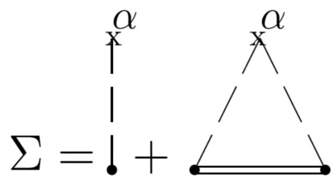

FIG. 2. The Dyson equation for the irreducible self-energy in the self-consistent Born approximation. The double solid line symbolizes the exact electron Green's function.

B. AMRO in the self-consistent Born and noncrossing approximations

The analytical solution for the impurity-averaged electron Green's function in the potential of point-like randomly distributed impurities can be obtained in a strong magnetic field, when $\hbar\omega_c \gg \hbar/\tau, t_z$, so that one can consider a single LL [23,24,38,39]. If the short-range elastic impurities are taken into account in the self-consistent Born approximation (SCBA), shown in Fig. 2, the LL shape is a semicircle [23] (see also Eq. (22) of Ref. [37]):

$$D(E) = \frac{|\mathrm{Im}\,G(E)|}{\pi} = \frac{\sqrt{4\hbar\omega_c\Gamma_0/\pi - E^2}}{2\Gamma_0\hbar\omega_c} \equiv \frac{2}{\pi}\frac{\sqrt{\Gamma_B^2 - E^2}}{\Gamma_B^2}, \tag{25}$$

where the energy $E = \varepsilon - \epsilon_{n_F} - n_i U$ is counted from the highest occupied LL n_F, shifted by the average impurity potential $n_i U$, where n_i is the 3D impurity concentration and U is the strength of each short-range impurity potential $V_i(\boldsymbol{r}) = U\delta^3(\boldsymbol{r} - \boldsymbol{r}_i)$. The noncrossing approximation, which includes the summation of all diagrams without intersection of impurity lines, improves the self-consistent Born approximation by replacing the Born scattering amplitude by the total scattering amplitude on each impurity (see Fig. 3). This improvement is important only when the scattering amplitude by each impurity $a \equiv mU/2\pi\hbar^2$ is larger than the interlayer distance d. The noncrossing approximation gives a slightly asymmetric but also a dome-like DoS shape [24]:

$$D(E) = \frac{\sqrt{(E - E_1)(E_2 - E)}}{2\pi\,|E_g\,(E + c_i E_g)|}. \tag{26}$$

Equation (26) is identical to Eq. (2.11) of Ref. [24] with slightly different notation of $E = \varepsilon - \epsilon_{n_F} - n_i U = \varepsilon - \epsilon_{n_F} - c_i E_g$. As in Ref. [24], $E_g = V_0/2\pi l_H^2$ is the normalized strength of the point-like impurity potential, $V_0 = U|\psi(z_i)|^2$ is the 2D analogue of the 3D strength U of the point-like impurity potential: $V_i(x,y) = V_0\delta(x - x_i)\delta(y - y_i)$, $\psi(z_i)$ is the value of the out-of-plane electron wave function at the impurity position z_i, and the dimensionless quantity c_i is the ratio of impurity concentration to the electron density on one LL per one spin component:

$$c_i = n_i d/g_{LL} = 2\pi l_H^2 n_i d. \tag{27}$$

The boundaries of the DoS dome in Eq. (26) are given by

$$E_1 = E_g(1 - 2\sqrt{c_i}), \quad E_2 = E_g(1 + 2\sqrt{c_i}). \tag{28}$$

Both in the self-consistent Born and in noncrossing approximations the LL half-width is

$$\Gamma_B \equiv (E_2 - E_1)/2 = 2E_g\sqrt{c_i} = \sqrt{4\hbar\omega_c\Gamma_0/\pi} \propto \sqrt{B_z}, \tag{29}$$

and the boundaries of the DoS of each LL are sharp. At $c_i \gg 1$, which corresponds to the typical experimental situation in various systems including high-T_c layered superconductors, both the SCBA and noncrossing approximations give the same DoS. This can be proved by taking the limit $c_i \gg 1$ in Eq. (26), which gives Eq. (25) after making use the notations in Eq. (29). Therefore, below we calculate AMRO for the symmetric DoS in Eq. (25).

The crossover from the low-field value Γ_0 to high-field dependence Γ_B of the LL width in Eq. (29) and the similar crossover of the interlayer MR were studied in Ref. [37] in SCBA. Within the SCBA this crossover is sharp and takes place at $\hbar\omega_c = \pi\Gamma_0$.

Due to the dependence $V_0 = U|\psi(z_i)|^2$, in addition to the integration over x_i and y_i, averaging over the impurity positions $r_i = \{x_i, y_i, z_i\}$ also includes the integration over z_i, which is approximately equivalent to the integration over the weighted strength V_0 of each impurity [41,42]. This lifts the LL degeneracy even at low impurity concentration, because there are still many impurities at a large distance from the electron state, which produce a weak scattering potential. In addition, this may change the LL shape, especially at low impurity concentration [41]. However, to consider this effect one also needs the impurity distribution function $n_i(z)$ in the interlayer direction, which is usually unknown. Below we consider the case of large impurity concentration $n_i > 1/2\pi l_H^2 d$, equivalent to $c_i > 1$, when one can keep only the impurities within the conducting layers. These impurities produce almost equal 2D scattering potential of the strength $V_0 \approx U|\psi(0)|^2 \approx U/d$, and one can use Eq. (25) without additional integration over z_i.

At $\hbar\omega_c > 2\Gamma_B$, i.e., when the LLs do not overlap and Eq. (25) is valid, substituting Eq. (25) into Eq. (19) we find that the sum over p in Eq. (19) contains only one term $p = 0$. All other terms with $p \neq 0$ vanish, because the product $\mathrm{Im}G(\varepsilon,n)\mathrm{Im}G(\varepsilon,n+p) = 0$ for $p \neq 0$ gives the overlap of different LLs. At $\hbar\omega_c > 2\Gamma_B$ and $n_{LL}^F \gg 1$, substituting Eq. (16) into Eq. (19) we obtain a simple formula for AMRO:

$$\frac{\sigma_{zz}(\varepsilon,\theta)}{\sigma_{zz}^0} = \frac{2\Gamma_0\hbar\omega_c}{\pi} J_0^2(\kappa) \sum_{n\in Z} [\mathrm{Im}G(\varepsilon,n)]^2. \tag{30}$$

At $\hbar\omega_c \ll T \ll \mu$, when the MQO are damped by temperature, substituting Eqs. (25), (30), and (29) into Eq. (21) and performing the integration over E,

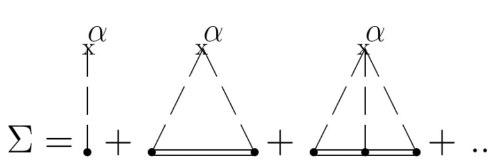

FIG. 3. The Dyson equation for the irreducible self-energy, corresponding to the noncrossing (self-consistent single-site) approximation. The double solid line symbolizes the exact electron Green's function.

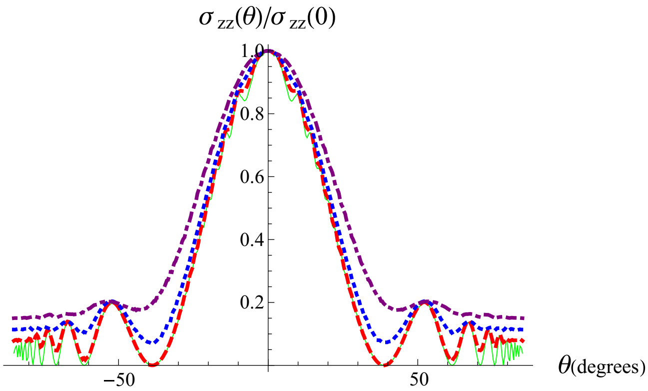

FIG. 4. (Color online) AMRO for the same parameters as in Fig. 1 but for the dome-shaped DoS of LLs, corresponding to the self-consistent Born approximation and given by Eq. (25). The AMRO are much stronger than for the Lorentzian LL shape, shown in Fig. 1.

we obtain

$$\frac{\bar{\sigma}_{zz}(\mu)}{\sigma_{zz}^{0}} = J_0^2(\kappa)\,\frac{2\Gamma_0\hbar\omega_c}{\pi}\int_{-\Gamma_B}^{\Gamma_B}\frac{4dE}{\hbar\omega_c}\left(\frac{\sqrt{\Gamma_B^2-E^2}}{\Gamma_B^2}\right)^2$$
$$= J_0^2(\kappa)\,\frac{2\Gamma_B}{\hbar\omega_c}\frac{4}{3} = \frac{16\,J_0^2(\kappa)}{3\sqrt{\pi}}\sqrt{\frac{\Gamma_0}{\hbar\omega_c}}. \qquad (31)$$

At low temperature $T \ll \hbar\omega_c$ the sum over n in Eq. (30) reduces to one term $n = n_{LL}^{F}$, corresponding to the last occupied LL for each spin component, because other terms with $n \neq n_{LL}^{F}$ acquire an exponentially small factor $n_F'(\varepsilon)$ after substitution into Eq. (18).

Angular dependence of interlayer conductivity for the dome-like LL shape, calculated numerically using Eqs. (18) and (19), is shown in Fig. 4.

C. AMRO for Gaussian LL shape

The sharp boundaries in Eqs. (25) and (26) are not physical, being the consequence of the noncrossing approximation. Unlike the 3D case, in 2D this approximation does not have a rigorous substantiation. However, the calculations which take into account the diagrams with intersection of impurity lines [38], as well as the nonperturbative solutions [39,42,43,45], show that the neglected diagrams with intersection of impurity lines only produce the exponentially decreasing tails of the DoS dome given by Eqs. (25) or (26). In particular, the solution of self-consistent equations containing the diagrams of point-like impurity scattering for up to four impurity sites [38] gives the DoS a shape intermediate between dome-like (obtained in SCBA) and Gaussian (see Fig. 7 of Ref. [38]). The width of such a quasi-Gaussian LL shape follows Eq. (29) in a strong magnetic field. For the ground LL the Gaussian LL shape for the short-range disorder was confirmed by nonperturbative solutions [39]. However, according to the calculation in Ref. [38], with the increase of LL number n the contribution of diagrams with the intersection of impurity lines from m sites becomes smaller according to $(2n)^{-(m-1)}$. Thus, for high Landau levels and point-like impurities the SCBA gives quite accurate results. The exponential tails of the DoS per each LL contain only a small part of the total DoS and, hence, only slightly affect the interlayer conductivity, calculated in Sec. III B. The interparticle interaction may additionally modify the DoS shape, e.g., increasing the DoS tails. This is an open question yet, and in metals with many filled LLs the electron-electron interaction is assumed to be small.

At finite range of impurities the LL shape is closer to Gaussian. For a Gaussian correlator of the disorder potential $U(\mathbf{r})$, $\langle U(\mathbf{0})\,U(\mathbf{r})\rangle \propto \exp\left(-r^2/2d^2\right)$ with $d \gg l_H$, nonperturbative theory predicts the Gaussian LL shape (see Eqs. (41) and (5) of Ref. [45]; for a review see also Ref. [44]):

$$|\mathrm{Im}G(\varepsilon,n)| = (\sqrt{2\pi}/\Gamma)\exp[-2(\varepsilon-\epsilon_n)^2/\Gamma^2]. \qquad (32)$$

The LL width Γ may depend on magnetic field and even on the LL number n for various models of disorder. At $d \ll R_c \sim l_H\sqrt{2n_{LL}^F+1}$ and in a strong magnetic field $\Gamma = \Gamma(B_z)$ is still given by Eq. (29), while at $d \gg R_c$ the LL width Γ in Eq. (32) is approximately independent of B [45]. If disorder on adjacent conducting layers is uncorrelated, i.e., it is short-range in the z direction, and the in-plane electron Green's function is given by Eq. (7), the formulas derived in Sec. II remain valid, and one can use the Gaussian Green's function given by Eq. (32) to calculate the interlayer conductivity. Although the Gaussian LL shape has never been derived theoretically for high LLs and short-range disorder, for completeness, in this section we analyze the angular dependence of interlayer conductivity also for the Gaussian LL shape given by Eq. (32).

At $\hbar\omega_c \ll T \ll \mu$, i.e. when the MQO are damped by temperature or by the long-range variations of the chemical potential, we can obtain an analytical formula for AMRO, similar to Eq. (2) but for Gaussian LL shape. Substituting Eq. (32) into Eq. (22) and taking the integral

$$\int_{-\infty}^{\infty} dE\,|\mathrm{Im}G(E)|\,|\mathrm{Im}G(E+p\hbar\omega_c)|$$
$$= \int_{-\infty}^{\infty} dE\,\frac{2\pi}{\Gamma^2}\exp\left[-\frac{2E^2}{\Gamma^2}-\frac{2(E+p\hbar\omega_c)^2}{\Gamma^2}\right]$$
$$= \frac{\pi\sqrt{\pi}}{\Gamma}\exp\left[-\frac{(p\hbar\omega_c)^2}{\Gamma^2}\right]$$

we obtain

$$\frac{\bar{\sigma}_{zz}}{\sigma_{zz}^{0}} = \frac{2\sqrt{\pi}\Gamma_0}{\Gamma}\sum_{p=-\infty}^{\infty} J_p^2(\kappa)\exp\left[-\frac{(p\hbar\omega_c)^2}{\Gamma^2}\right]. \qquad (33)$$

For short-range disorder at $\hbar\omega_c \gg \Gamma_0 = \hbar/2\tau_0$, $\Gamma = \Gamma_B \propto \sqrt{B_z}$ is given by Eq. (29), and Eq. (33) becomes

$$\frac{\bar{\sigma}_{zz}}{\sigma_{zz}^{0}} = \frac{\pi}{\sqrt{2\omega_c\tau_0}}\sum_{p=-\infty}^{\infty} J_p^2(\kappa)\exp\left[-\frac{\pi p^2\omega_c\tau_0}{2}\right], \qquad (34)$$

where $\omega_c = \omega_{c0}\cos\theta$. If Γ in Eqs. (32) and (33) is independent of B_z, from Eq. (33) one obtains

$$\frac{\bar{\sigma}_{zz}(\theta)}{\bar{\sigma}_{zz}(\theta=0)} = \sum_{p=-\infty}^{\infty} J_p^2(\kappa)\,e^{-(2p\omega_c\tau)^2}. \qquad (35)$$

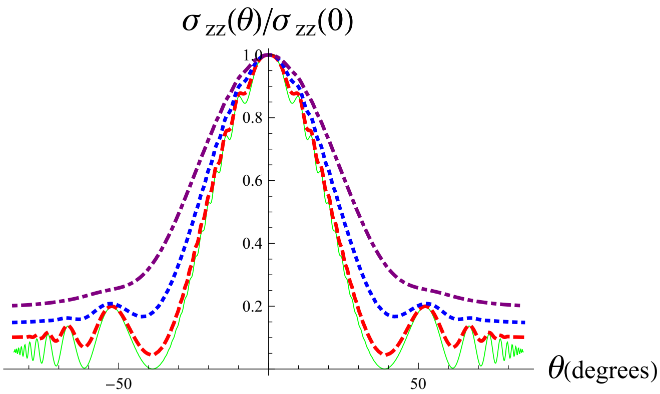

FIG. 5. (Color online) The same as in Figs. 1 and 4 but for Gaussian LL shape. The AMRO are much stronger, and the saturation value of σ_{zz} at $\theta \to \pm 90^\circ$ is considerably smaller than for the Lorentzian LL shape.

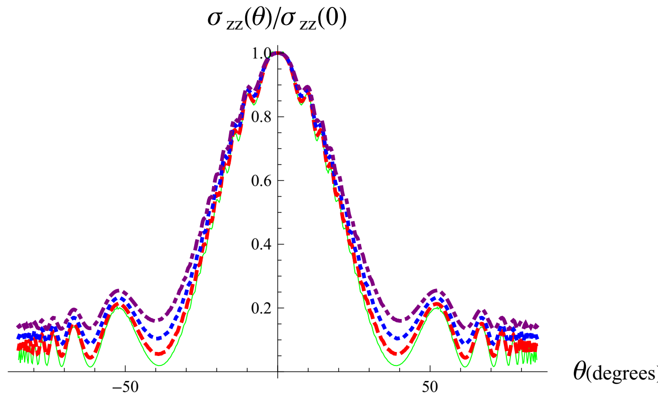

FIG. 6. (Color online) The angular dependence of normalized interlayer conductivity, calculated using Eqs. (18)-(19) for the Lorentzian LL shape with four different values of $\Gamma_0 = \hbar/2\tau$, which are 10 times less than in Figs. 1, 4 and 5: $\Gamma_0 = 0.05$ K (thin solid green curve), $\Gamma_0 = 0.15$ K (dashed red curve), $\Gamma_0 = 0.3$ K (dotted blue curve), and $\Gamma_0 = 0.5$ K (dash-dotted purple curve). The other parameters are the same as in Figs. 1,4 and 5: $k_F d = 3$, $\mu = 605K$, $T = 3$ K, and $B_0 \approx 11.6$ T, which for cyclotron mass $m^* = m_e$ and for $\theta = 0$ corresponds to $\hbar\omega_c = 10$ K.

In both cases, for Gaussian LL shape the damping of $p \neq 0$ terms is exponential and much stronger than the quadratic damping given by Eq. (2) for the Lorentzian LL shape.

At $\Gamma \ll \hbar\omega_c \ll T \ll \mu$, neglecting all exponentially small terms in Eq. (33) and substituting Eq. (29), we obtain

$$\bar{\sigma}_{zz}/\sigma_{zz}^0 = \pi J_0^2(\kappa)\sqrt{\Gamma_0/\hbar\omega_c}, \tag{36}$$

which is very close to Eq. (31) for a dome-like LL shape.

In Fig. 5 we plot the calculated AMRO for the Gaussian LL shape for four different values of $\Gamma_0 = \hbar/2\tau_0 = 0.5$, 1.5, 3.0, and 5.0 K, corresponding to $\omega_c\tau_0 = 10$, 3.33, 1.67, and 1.0 respectively at $\theta = 0$. Comparing Figs. 4 and 5 one sees that the AMRO for these two shapes are very close. Because of the sharp edges of the dome-like LL shape, the corresponding AMRO are slightly stronger for the same values of $\omega_c\tau_0$. However, the tails of the Gaussian LLs are exponentially small, which diminishes the difference between AMRO in Figs. 4 and 5. Since the Gaussian and dome-like LL shapes give quite close results for AMRO, the simple analytical formula in Eq. (33) for AMRO derived for Gaussian LL shape can be approximately applied for dome-shaped LLs with the same width.

On the other hand, the comparison of Fig. 1 with Figs. 4 and 5 shows that for the Lorentzian LL shape the same value of Γ_0 suppresses AMRO much stronger. In particular, at finite $\Gamma \lesssim \hbar\omega_c$ the minima of conductivity at the Yamaji angles are much deeper for the dome-like and Gaussian LL shapes than for the Lorentzian shape. Moreover, the minima of conductivity quickly tend to saturation with increasing of $\omega_c\tau$ in Figs. 4 and 5, while for Lorentzian LL shape in Fig. 1 this saturation is very slow. This difference can be easily understood by comparing the analytical formulas (2), (31), and (34) for AMRO at various LL shapes. This difference between AMRO for Lorentzian and Gaussian or dome-like LL shapes cannot be attributed to the different definitions of Γ_0. To illustrate this, in Fig. 6 we plot AMRO for Lorentzian LL shape for several values of $\Gamma_0 = 0.05$, 0.15, 0.3, and 0.5 K, which are 10 times smaller than those in Figs. 1, 4, and 5 and correspond to $\omega_c\tau_0 = 100$, 33.3, 16.7, and 10. We see that even the tenfold increase of $\omega_c\tau_0$ does not countervail the difference between the Lorentzian and the Gaussian or dome-like LL shapes. On the other hand, the twofold decrease of Γ is more than enough to make the Lorentzian DoS maximum narrower than the dome-like or Gaussian DoS maxima (see Fig. 7). Disregarding the shown dependence of AMRO amplitude on the LL shape may lead to the incorrect determination of $\omega_c\tau$ from the experimental data on AMRO.

To illustrate this point further, in Fig. 8 we plot the conductivity $\bar{\sigma}_{zz}(\theta_{Yam})/\sigma_{zz}(\theta = 0)$, calculated from Eqs. (2) and (33), in the first Yamaji angle θ_{Yam} (conductivity minimum) as function of $\omega_c\tau_0$ for the Lorentzian (solid green curve) and Gaussian (dashed red curve) LL shapes. The dotted blue curve gives the same ratio $\bar{\sigma}_{zz}(\theta_{Yam})/\sigma_{zz}(\theta = 0)$ for the

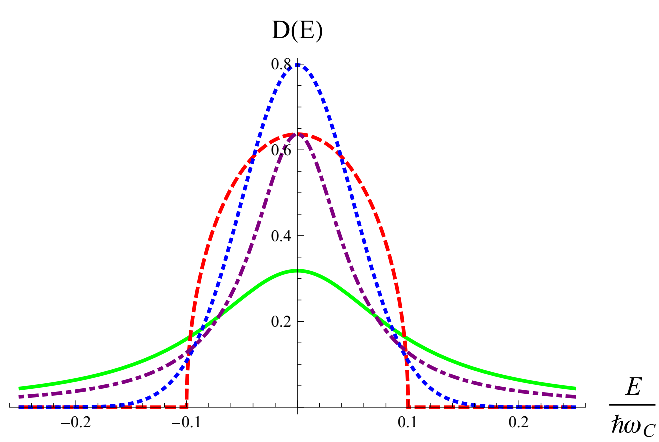

FIG. 7. (Color online) The normalized DoS at $\hbar\omega_c/\Gamma = 10$ for various LL shapes: Lorentzian given by Eq. (23) (solid green curve), dome-like given by Eq. (25) (dashed red curve), and Gaussian given by Eq. (32) (dotted blue curve). The dash-dotted purple curve gives the normalized DoS for Lorentzian LL shape at twice larger value $\hbar\omega_c/\Gamma = 20$.

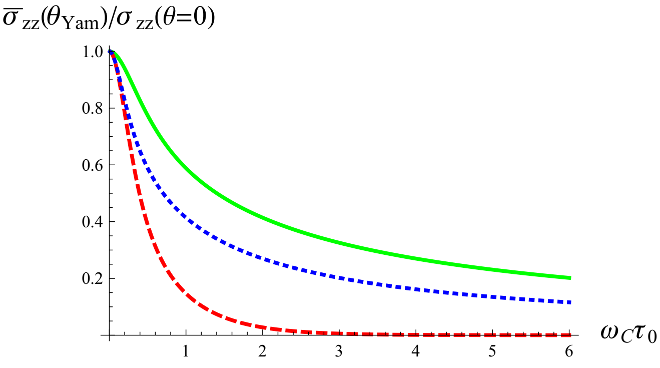

FIG. 8. (Color online) Calculated value of conductivity $\bar{\sigma}_{zz}(\theta_{Yam})/\sigma_{zz}(\theta=0)$ in the first Yamaji angle θ_{Yam} (conductivity minimum) as function of $\omega_c\tau$ for the Lorentzian (solid green curve) and Gaussian (dashed red curve) LL shapes. The dotted blue curve gives the solid green curve twice shrunk along the abscissa axis, which corresponds to $\bar{\sigma}_{zz}(\theta_{Yam})/\sigma_{zz}(\theta=0)$ for Lorentzian LL shape at twice smaller Γ_0 value in the same magnetic field.

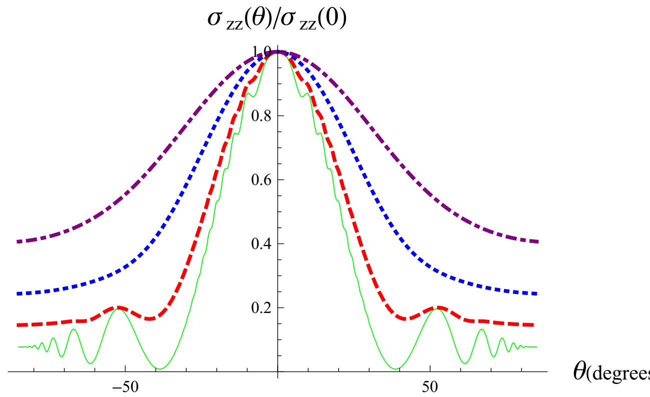

FIG. 9. (Color online) The angular dependence of normalized interlayer conductivity, calculated using Eqs. (18) and (19) for the Gaussian LL shape with four values of $\Gamma_0 = \hbar/2\tau_0$, which are $2\sqrt{\pi}$ times greater than in Figs. 1, 4, and 5: $\Gamma_0 = \sqrt{\pi}$ K (thin solid green curve), $\Gamma_0 = 3\sqrt{\pi}$ K (dashed red curve), $\Gamma_0 = 6\sqrt{\pi}$ K (dotted blue curve), and $\Gamma_0 = 10\sqrt{\pi}$ K (dash-dotted purple curve). The other parameters are the same as in Figs. 1, 4, and 5: $k_F d = 3$, $\mu = 605$ K, $T = 3$ K, and $B_0 \approx 11.6$ T, which for cyclotron mass $m^* = m_e$ and for $\theta = 0$ corresponds to $\hbar\omega_c = 10$ K.

Lorentzian LL shape but for a twice larger value of $\omega_c\tau_0$ (twice shrunk along the abscissa axis). We see that the change from Lorentzian to Gaussian LL shape has much stronger effect on AMRO than the two-times increase of $\omega_c\tau_0$.

Using the identity $\sum_{p=-\infty}^{\infty} J_p^2(\kappa) = 1$, at zero field $\hbar\omega_c/\Gamma = 0$ from Eq. (33) one obtains $\bar{\sigma}_{zz}(B=0)/\sigma_{zz}^0 = 2\sqrt{\pi}\Gamma_0/\Gamma$. Since without a magnetic field one expects $\bar{\sigma}_{zz}(\theta=0) = \sigma_{zz}^0$, for consistency one naively could write $\Gamma(B=0) = 2\sqrt{\pi}\Gamma_0$, which implies that the change of the electron DoS from Lorentzian given by Eq. (23) to Gaussian given by Eq. (32) must be accompanied by the $2\sqrt{\pi}$-times increase of the zero-field level broadening Γ_0. The angular dependence of MR for a Gaussian LL with $2\sqrt{\pi}$ -times increased Γ_0 value becomes much closer to that for a Lorentzian LL shape (compare Figs. 9 and 1), and only the Yamaji minima of conductivity are still much sharper for Gaussian LL shape at $\omega_c\tau_0 > 1$. However, this renormalization of Γ_0 is not correct, because the condition $\bar{\sigma}_{zz}(\theta=0) = \sigma_{zz}^0$ with σ_{zz}^0 given by Eq. (3) assumes Lorentzian DoS, while Eq. (33) is derived only for Gaussian broadening of electron levels. In a weak magnetic field $\omega_c\tau_0 \ll 1$, even at $t_z \ll \hbar\omega_c$, the LL shape is not Gaussian but closer to Lorentzian, because $\Sigma(\varepsilon) \approx$ const [26,37]. Hence, in addition to the dependence $\Gamma(B_z)$, the increase of magnetic field in quasi-2D metals leads to the crossover of the LL shape from Lorentzian to Gaussian.

At $\Gamma \ll \hbar\omega_c$, Eqs. (33)–(35) give exponentially small values of $\sigma_{zz}^G \sim \sigma_{zz}^0 \exp[-(\hbar\omega_c/2\Gamma)^2]$ in the Yamaji angles. However, in experiments the interlayer conductivity in the Yamaji angles may saturate at finite value with increasing magnetic field. Besides the finite LL broadening Γ, MR in the Yamaji maxima is limited by the additional "incoherent" mechanisms of interlayer transport, such as interlayer hopping via resonance impurities [47–49] and dislocations, or boson-assisted tunneling [50,51]. Approximately, the contribution of the incoherent channels to σ_{zz} does not depend on the tilt angle θ of the magnetic field and gives a constant upward shift of the curves in Figs. 1, 4–6, 8, and 9. These incoherent channels determine the interlayer conductivity at the Yamaji angles in a very strong magnetic field. However, the incoherent channels of interlayer electron transport may depend on the B_z component of the magnetic field if they involve the in-plane electron motion, as in the model of Ref. [47].

IV. HIGH TILT ANGLE

From Figs. 1 and 5 one observes that not only the AMRO amplitude but also the ratio $\sigma_{zz}(\theta \to \pm 90^\circ)/\sigma_{zz}(\theta=0)$ depend on the LL shape: the saturation value of σ_{zz} at $\theta \to \pm 90^\circ$ looks considerably smaller for the Gaussian LL shape than for the Lorentzian. However, the calculated absolute values of $\sigma_{zz}(\theta \to \pm 90^\circ)/\sigma_{zz}^0$ depend only on $\omega_{c0}\tau \cdot k_F d$ but not on the LL shape. These values agree well with Eq. (10) of Ref. [21], which predicts

$$\sigma_{zz}(\theta \to \pm 90^\circ)/\sigma_{zz}^0 = 1/\sqrt{1+(k_F d\omega_{c0}\tau)^2}, \tag{37}$$

where $\omega_{c0} = eB_0/m^* c$. In Ref. [21], Eq. (37) was obtained in the τ approximation using the quasiclassical electron trajectories along the well-defined 3D Fermi surface. The τ approximation does not work in a strong perpendicular-to-layers magnetic field, but it may work properly when the magnetic field is along the conducting layers so that $B_z \to 0$. One can also expect that the LL shape is not important in the limit $\theta \to \pm 90^\circ$ and $B_z \to 0$. To check this, we now calculate $\sigma_{zz}(\theta \to \pm 90^\circ)/\sigma_{zz}^0$ for the Lorentzian and Gaussian LL shapes without the use of a 3D Fermi surface and of the τ-approximation.

At high tilt angle the argument of the Bessel's functions in Eq. (16) $\kappa \equiv k_F d \tan\theta \gg 1$, and one can use its asymptotic expansion, which gives

$$\begin{aligned} Z(n,p) &\approx (2/\pi\kappa)\cos^2(\kappa - \pi p/2 - \pi/4) \\ &= [1+\cos(2\kappa - \pi p - \pi/2)]/\pi\kappa. \end{aligned} \tag{38}$$

The square brackets contain a sum of the monotonic and alternating terms as a function of p. At $B_z \to 0$, when the LL separation $\hbar\omega_c \ll \Gamma$, the factor $\mathrm{Im}\, G(\varepsilon, n+p)$ in Eq. (19) depends very weakly on p, and the alternating term gives a negligible contribution to Eq. (19). Substituting only a constant term from Eq. (38) into Eq. (19) gives at $\theta \to \pm 90^\circ$

$$\frac{\sigma_{zz}(\varepsilon)}{\sigma_{zz}^0} \approx \frac{2\Gamma_0 \hbar\omega_c}{\pi^2 \kappa} \sum_{n,p\in Z} \mathrm{Im}G(\varepsilon,n)\mathrm{Im}G(\varepsilon,n+p). \quad (39)$$

At $\hbar\omega_c \equiv \hbar e B_z/m^* c \ll \Gamma$ one can replace the summations over n and p by the integrations. For the Lorentzian LL shape this gives

$$\frac{\sigma_{zz}(\varepsilon)}{\sigma_{zz}^0} \approx \int\int_{-\infty}^{\infty} \frac{dpdn\Gamma_0\hbar\omega_c\Gamma^2(2/\pi^2\kappa)}{[(\epsilon-\epsilon_n)^2+\Gamma^2][(\epsilon-\epsilon_{n+p})^2+\Gamma^2]}$$
$$= 2\Gamma_0/\kappa\hbar\omega_c = (\omega_{c0}\tau_0 k_F d)^{-1} \quad (40)$$

in agreement with Eq. (14) of Ref. [22]. For Gaussian LL shape at $\theta \to \pm 90^\circ$ we obtain the same result:

$$\frac{\sigma_{zz}(\varepsilon)}{\sigma_{zz}^0} \approx \frac{2\Gamma_0\hbar\omega_c}{\pi\kappa\Gamma^2} \int_{-\infty}^{\infty} dn \exp\left[-\frac{(\epsilon-\epsilon_n)^2}{\Gamma^2}\right]$$
$$\times \int_{-\infty}^{\infty} dp \exp\left[-\frac{(\epsilon-\epsilon_{n+p})^2}{\Gamma^2}\right] = \frac{2\Gamma_0}{\kappa\hbar\omega_c}. \quad (41)$$

Thus, the ratio $\sigma_{zz}(\theta \to \pm 90^\circ)/\sigma_{zz}^0 = (\omega_{c0}\tau k_F d)^{-1}$ is the same for Lorentzian and Gaussian LL shapes. This result is natural, because when $\theta \to \pm 90^\circ$ and B_z is small, so that $\Gamma \gg \hbar\omega_c$, the LLs are smeared and their shape is not important. However, $\sigma_{zz}^0 \neq \sigma_{zz}(\theta = 0)$, and $\sigma_{zz}(\theta = 0)$ depends on the LL shape.

At $\Gamma_0 \ll \hbar\omega_c \ll T \ll \mu$, substituting Eq. (23) to Eqs. (20) and (21) and taking the integral

$$\int_{-\frac{\hbar\omega_c}{2}}^{\frac{\hbar\omega_c}{2}} \frac{dE}{\hbar\omega_c} |\mathrm{Im}G(E)|^2 = \int_{-\infty}^{\infty} \frac{dE}{\hbar\omega_c} \frac{\Gamma^2}{(E^2+\Gamma^2)^2} = \frac{\pi/2}{\hbar\omega_c\Gamma},$$

we obtain at $\Gamma = \Gamma_B = \sqrt{4\hbar\omega_c\Gamma_0/\pi}$ for the Lorentzian LL shape

$$\frac{\bar\sigma_{zz}}{\sigma_{zz}^0} = J_0^2(\kappa)\frac{\Gamma_0}{\Gamma} = J_0^2(\kappa)\frac{\sqrt{\pi}}{2}\sqrt{\frac{\Gamma_0}{\hbar\omega_c}}, \quad (42)$$

which is $2\sqrt{\pi} \approx 3.5$ times smaller than in Eqs. (33) and (36) for Gaussian LL shape. Therefore, in Fig. 5 the ratio $\sigma_{zz}(\theta = 0)/\sigma_{zz}(\theta \to \pm 90^\circ)$ is $2\sqrt{\pi}$ times larger than in Fig. 1. In a weak magnetic field, i.e., at $\hbar\omega_c \ll \Gamma_0$, for all LL shapes $\sigma_{zz}(\theta = 0) = \sigma_0$. In a strong magnetic field, i.e., at $\hbar\omega_c \gg \Gamma_0$, again for all three LL shapes $\bar\sigma_{zz}(\theta = 0)/\sigma_0 = C/\sqrt{\omega_c\tau_0}$, but the numerical coefficient C in this dependence is different for different LL shapes. Therefore, the decrease of $\bar\sigma_{zz}(B_z)$ is faster for the Gaussian and dome-like than for Lorentzian LL shapes. The crossover from weak to strong-field behavior of $\bar\sigma_{zz}(B_z)$ in SCBA at $\theta = 0$ was studied numerically in Ref. [37].

In Fig. 6 $\omega_c\tau_0$ is 10 times larger than in Fig. 1. However, contrary to Eqs. (37) and (40), the ratio $\sigma_{zz}(\theta = 0)/\sigma_{zz}(\theta \to \pm 90^\circ)$ in Fig. 6 is only $\sqrt{10}$ times larger than in Fig. 1, because the value $\sigma_{zz}(\theta = 0) \propto 1/\sqrt{\omega_c\tau_0}$. For this reason, the ratio $\sigma_{zz}(\theta = 0)/\sigma_{zz}(\theta \to \pm 90^\circ)$ in Figs. 9 and 1 is different in spite of the $2\sqrt{\pi}$-times increased Γ_0 value in Fig. 9.

On experiment one can measure both the ratios $\sigma_{zz}(\theta = 0)/\sigma_{zz}(\theta \to \pm 90^\circ)$ and $\sigma_{zz}(\theta \to \pm 90^\circ)/\sigma_{zz}^0$, which also provides the information about the LL shape. The value $k_F d$ is usually known from the AMRO period, and ω_{c0} (determined by the effective mass m^*) is known from the MQO period. Hence, the experimentally obtained ratio $\sigma_{zz}(\theta \to \pm 90^\circ)/\sigma_{zz}^0$ provides a tool to determine τ_0 with high accuracy, which may considerably differ from the τ value obtained from the Dingle temperature.

V. SPIN CURRENT AND THE INFLUENCE OF ZEEMAN SPLITTING ON AMRO

The spin current, being a key object of spintronics, attracts a great attention for its present-day and potential applications (see, e.g., Refs. [52,53] for reviews). In our system, the nonzero spin current conductivity $s_{zz} \equiv \sigma_{zz\uparrow} - \sigma_{zz\downarrow}$ appears because the electrons with opposite spin orientations give nonequal contributions to σ_{zz}. The Fermi energy of spin-up and -down electrons differs by the Zeeman energy $g\mu_B B$, which leads to nonequal values of k_F and κ in Eqs. (2), (16), and (33)–(36) and, hence, to different angular dependence of conductivity for opposite spin orientations. The corresponding difference $\delta\kappa$ in the argument of the Bessel functions in Eq. (16) is

$$\delta\kappa = g\mu_B B_0 \tan\theta\, d/\hbar v_F \approx 2\mu_B B_0 m^* d \tan(\theta)/(\hbar^2 k_F). \quad (43)$$

The monotonic part $\bar s_{zz}$ of the spin-current conductivity, determined as the difference between the monotonic parts of conductivities with spin up and down as

$$\bar s_{zz} = \bar\sigma_{zz}(\mu + g\mu_B B) - \bar\sigma_{zz}(\mu) = \bar\sigma_{zz}(\kappa + \delta\kappa) - \bar\sigma_{zz}(\kappa), \quad (44)$$

for the Lorentzian LL shape in the first order in $\kappa \ll 1$ is given by

$$\frac{\bar s_{zz}}{\sigma_{zz}^0} \approx \left\{2J_0(\kappa)J_0'(\kappa) + 4\sum_{\nu=1}^{\infty}\frac{[J_\nu(\kappa)J_\nu'(\kappa)]}{1+(\nu\omega_c\tau)^2}\right\}\delta\kappa$$
$$= -\delta\kappa \sum_{\nu=-\infty}^{\infty} \frac{J_\nu(\kappa)[J_{\nu+1}(\kappa) - J_{\nu-1}(\kappa)]}{1+(\nu\omega_c\tau)^2}, \quad (45)$$

where we have applied $2J_\nu'(\kappa) = J_{\nu-1}(\kappa) - J_{\nu+1}(\kappa)$. In a field $B_0 = 10$ T and for the parameters $d = 20$ Å, $k_F = 0.14$ Å^{-1}, and $m^* \approx 2m_e$, corresponding to the organic metal α-(BEDT-TTF)$_2$KHg(SCN)$_4$ (see Ref. [54]), $\delta\kappa \approx 0.1\tan\theta$ is not negligible. For these parameters, in Fig. 10 we plot the angular dependence of $\bar s_{zz}/\sigma_{zz}^0$, calculated without expansion in $\delta\kappa$, i.e., from Eqs. (44) and (2), corresponding to the Lorentzian LL shape with three different values of Γ, independent of B_z and corresponding to $\omega_c\tau = 10$ (solid green line), 1 (dashed red line), and 0.5 (dotted blue line). We also checked that the first-order expansion in $\delta\kappa \approx 0.1\tan\theta$, given by Eq. (45), works very well for $|\theta| < 86^\circ$.

In the Yamaji angles $\sigma_{zz}(\theta)/\sigma_{zz}^0 \ll 1$, and the spin current for these angles can be comparable to the charge current, being also considerably smaller than for other angles at $\omega_c\tau \gg 1$.

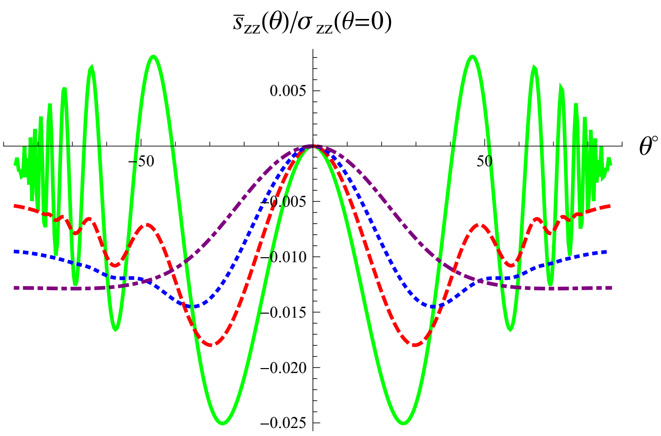

FIG. 10. (Color online) The angular dependence of the monotonic part of the spin-current conductivity $\bar{s}_{zz}/\sigma_{zz}^0$, calculated from Eq. (44) for Lorentzian LL shape with four different values of $\omega_c\tau_0 = 10$ (solid green line), 2.0 (dashed red line), 1.0 (dotted blue line), and 0.5 (dash-dotted purple curve).

Note that at $\omega_c\tau \gg 1$ the monotonic part of spin current changes sign in the proximity of the Yamaji angles from "−" to "+", and it changes its sign back in the extremum of $\sigma_{zz}(\theta)$. In heterostructures the spin current can be considerably larger than shown in Fig. 10, because of a larger value of $\delta\kappa$, which is proportional to the interlayer distance d.

For Gaussian and dome-like LL shapes the AMRO are sharper, and the spin current is larger than in Fig. 10. To show this, in Fig. 11 we plot the angular dependence of the spin current calculated using Eq. (34) for the same values of $\omega_c\tau$ as in Fig. 10. We see that the saturation of spin current as $\omega_c\tau$ increases is much faster for Gaussian LL shape, similar to the charge current AMRO. From Eqs. (44) and (33) for the Gaussian LL shape and $\delta\kappa \ll 1$ we obtain the analytical formula for the spin current [compare to Eq. (45)]

$$\frac{\bar{s}_{zz}}{\sigma_{zz}^0} \approx \delta\kappa \frac{4\sqrt{\pi}\Gamma_0}{\Gamma} \sum_{\nu=-\infty}^{\infty} J_\nu(\kappa) J_\nu'(\kappa) \exp\left[-\frac{(\nu\hbar\omega_c)^2}{\Gamma^2}\right]. \tag{46}$$

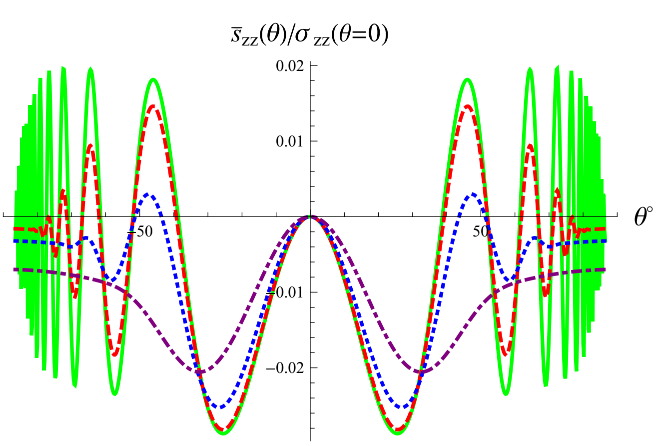

FIG. 11. (Color online) The angular dependence of the monotonic part of the spin-current conductivity $\bar{s}_{zz}/\sigma_{zz}^0$, calculated from Eq. (34) for Gaussian LL shape with the same four different values as in Fig. 10 of $\omega_c\tau_0 = 10$ (solid green line), 2.0 (dashed red line), 1.0 (dotted blue line), and 0.5 (dash-dotted purple curve).

VI. CONCLUSIONS

In this paper we present the quantum-mechanical calculations of the angular dependence of interlayer magnetoresistance in quasi-2D layered metals. Most previous calculations of AMRO neglected the magnetic quantum oscillations (MQO) from the beginning [17,22], or even used the semiclassical Boltzmann transport equation in the constant-τ approximation [16,18–20]. However, even if MQO are not seen, being damped by temperature or long-range disorder, they may strongly influence the interlayer conductivity and its angular dependence in a strong magnetic field, when $\hbar\omega_c \gg t_z,\Gamma$ [29–32]. In the present theoretical study we take MQO into account and consider their influence on the angular dependence of interlayer conductivity. Our calculation is applicable for various shapes of the Landau levels, thus generalizing the calculations in Refs. [17,22,29]. This is important, because when the interlayer transfer integral t_z and the LL broadening Γ are less than the LL separation $\hbar\omega_c$, the LL shape is not Lorentzian [24,33,38–44] We also take into account the so-called "quantum term" in the magnetoresistance [25–27], originating from MQO and neglected in the previous studies [17,22,29].

Our calculation shows that the LL shape is important for the angular dependence of magnetoresistance. The AMRO amplitude is stronger for the Gaussian or dome-like LL shapes, corresponding to the microscopic models at $t_z \ll \Gamma \ll \hbar\omega_c$, than for traditionally used Lorentzian LL shape (compare Figs. 1 and 4 or 5). With increasing magnetic field, the saturation of interlayer conductivity values in the AMRO minima, corresponding to the Yamaji angles, is much faster for Gaussian or dome-like LL shapes than for Lorentzian (see Fig. 8). The ratio $\sigma_{zz}(\theta = 0)/\sigma_{zz}(\theta \to \pm 90^\circ)$ for the Gaussian or dome-like DoS is also several times larger than for Lorentzian LL shape. However, the ratio $\sigma_{zz}(\theta \to \pm 90^\circ)/\sigma_0$ does not depend on the LL shape and provides a tool to determine the zero-field mean free time value τ_0, which may considerably differ from the τ value obtained from the Dingle temperature. For arbitrary LL shape one can use Eqs. (18) and (19) with $Z(n,p)$ given by Eq. (12) or by Eqs. (15) or (16). At $\hbar\omega_c \ll T \ll \mu$ these formulas simplify to Eqs. (20)–(22). In the high-field limit, when the LL shape is not Lorentzian but closer to dome-like or Gaussian, we derive simple explicit formulas (33)–(36) for $\sigma_{zz}(\theta)$, which replace the traditionally used Eqs. (2)–(5) derived only for Lorentzian LL shape.

We also estimated the spin current, which appears because of AMRO. For typical parameters of the organic metal α-(BEDT-TTF)$_2$KHg(SCN)$_4$ and in the field $B \sim 10$ T the spin current is about 2% of the zero-field charge current [see Eqs. (45), (46) and Figs. 10, 11], but it may almost reach the charge current for special tilt angles of magnetic field. In heterostructures the spin current can be considerably larger. The angular oscillations of the spin current are stronger and shifted by the phase $\sim\pi/2$ as compared to the usual charge-current AMRO.

ACKNOWLEDGMENTS

The work was supported by the Russian Foundation for Basic Research Grant No. 13-02-00178 and by SIMTECH Program (Grant No. 246937).

APPENDIX A: CLASSICAL PART OF CONDUCTIVITY

Substituting Eq. (7) into the first line of Eq. (11) one obtains

$$\begin{aligned} Cl = \int dy_2 dy_1 dx_2 dx_1 \cos\left[q(y_2-y_1)\right] \\ \times \sum_{p,n,k_y,k_y'} \Psi^*_{n,k_y'}(r_1)\Psi_{n,k_y'}(r_2)G(\epsilon,n) \\ \times \Psi^*_{n+p,k_y}(r_2)\Psi_{n+p,k_y}(r_1)G^*(\epsilon,n+p), \end{aligned}$$

where the wave functions are given by Eqs. (9) and (10). Integration over y_2, y_1 (in a unit square) gives

$$\begin{aligned} Cl = 4\pi^2 \mathrm{Re} \int dx_2 dx_1 \sum_{p,n,k_y,k_y'} \Psi^*_{n+p}\left(x_2 - l_H^2 k_y\right) \\ \times \Psi_{n+p}\left(x_1 - l_H^2 k_y\right)\Psi^*_n\left(x_1 - l_H^2 k_y'\right)\Psi_n\left(x_2 - l_H^2 k_y'\right) \\ \times G^*(\epsilon,n+p)G(\epsilon,n)\delta(k_y+q-k_y'). \end{aligned} \tag{A1}$$

Summation over k_y' cancels the δ function. Then we use the identity

$$\begin{aligned} \int_{-\infty}^{\infty} dx\, e^{-c^2x^2} H_n(a+cx)H_{n+p}(b+cx) \\ = \frac{2^n\sqrt{\pi}n!b^p}{c} L_n^p(-2ab), \quad 0 \leqslant p. \end{aligned} \tag{A2}$$

Using Eqs. (A2) and (10) one may get

$$\begin{aligned} \int_{-\infty}^{\infty} dx \Psi_{n+p}\left(x - l_H^2 k_y\right)\Psi_n\left(x - l_H^2(k_y+q)\right) \\ = \exp\left(-\frac{(ql_H)^2}{4}\right)\left(\frac{ql_H}{\sqrt{2}}\right)^p L_n^p\left(\frac{(ql_H)^2}{2}\right)\sqrt{\frac{n!}{(n+p)!}}. \end{aligned} \tag{A3}$$

The integration over x_1,x_2 in Eq. (A1) is performed using Eq. (A3). Then, making the summation over k_y, which just gives the LL degeneracy $g_{LL} = 1/2\pi l_H^2 = eB_z/2\pi\hbar c$, we obtain Eq. (11).

APPENDIX B: QUANTUM PART OF CONDUCTIVITY

Substituting Eq. (7) into the first line of Eq. (13) gives

$$\begin{aligned} Q = \int dy_2 dy_1 dx_2 dx_1 \exp\left[iq(y_2-y_1)\right] \\ \times \sum_{p,n,k_y,k_y'} \Psi^*_{n,k_y'}(r_1)\Psi_{n,k_y'}(r_2)G(\epsilon,n) \\ \times \Psi^*_{n+p,k_y}(r_2)\Psi_{n+p,k_y}(r_1)G(\epsilon,n+p), \end{aligned}$$

which after the substitution of Eq. (9) and integration over y_1,y_2 becomes

$$\begin{aligned} Q = 4\pi^2 \mathrm{Re} \int dx_2 dx_1 \sum_{p,n,k_y,k_y'} \Psi^*_{n+p}\left(x_2 - l_H^2 k_y\right) \\ \times \Psi_{n+p}\left(x_1 - l_H^2 k_y\right)\Psi^*_n\left(x_1 - l_H^2 k_y'\right)\Psi_n\left(x_2 - l_H^2 k_y'\right) \\ \times G(\epsilon,n+p)G(\epsilon,n)\delta(k_y+q-k_y'). \end{aligned}$$

The integration over x_1,x_2 is similar to that in Eq. (A1) and can be easily done using Eq. (A3). Summation over k_y gives the LL degeneracy. Performing these integrations we obtain Eq. (13).

[1] M. V. Kartsovnik, Chem. Rev. **104**, 5737 (2004).
[2] J. Singleton, Rep. Prog. Phys. **63**, 1111 (2000).
[3] M. V. Kartsovnik and V. G. Peschansky, Low Temp. Phys. **31**, 185 (2005) [Fiz. Nizk. Temp. **31**, 249 (2005)].
[4] T. Ishiguro, K. Yamaji, and G. Saito, *Organic Superconductors*, 2nd ed. (Springer-Verlag, Berlin, 1998).
[5] J. Wosnitza, *Fermi Surfaces of Low-Dimensional Organic Metals and Superconductors* (Springer-Verlag, Berlin, 1996).
[6] J. S. Brooks, V. Williams, E. Choi1, D. Graf, M. Tokumoto, S. Uji, F. Zuo, J. Wosnitza, J. A. Schlueter, H. Davis, R. W. Winter, G. L. Gard, and K. Storr, New J. Phys. **8**, 255 (2006).
[7] *The Physics of Organic Superconductors and Conductors*, edited by A. G. Lebed, Springer Series in Materials Science, Vol. 110 (Springer-Verlag, Berlin, 2008).
[8] N. E. Hussey, M. Abdel-Jawad, A. Carrington, A. P. Mackenzie, and L. Balicas, Nature (London) **425**, 814 (2003).
[9] M. Abdel-Jawad, M. P. Kennett, L. Balicas, A. Carrington, A. P. Mackenzie, R. H. McKenzie, and N. E. Hussey, Nat. Phys. **2**, 821 (2006).
[10] M. Abdel-Jawad, J. G. Analytis, L. Balicas, A. Carrington, J. P. H. Charmant, M. M. J. French, and N. E. Hussey, Phys. Rev. Lett. **99**, 107002 (2007).
[11] Malcolm P. Kennett and Ross H. McKenzie, Phys. Rev. B **76**, 054515 (2007).
[12] T. Helm, M. V. Kartsovnik, I. Sheikin *et al.*, Phys. Rev. Lett. **105**, 247002 (2010).
[13] M. Kuraguchi, E. Ohmichi, T. Osada, and Y. Shiraki, Synthetic Met. **133-134**, 113 (2003).
[14] M. V. Kartsovnik, P. A. Kononovich, V. N. Laukhin, and I. F. Shchegolev, JETP Lett. **48**, 541 (1988).
[15] K. Yamaji, J. Phys. Soc. Jpn. **58**, 1520 (1989).
[16] R. Yagi, Y. Iye, T. Osada, and S. Kagoshima, J. Phys. Soc. Jpn. **59**, 3069 (1990).
[17] Yasunari Kurihara, J. Phys. Soc. Jpn. **61**, 975 (1992).
[18] M. V. Kartsovnik, V. N. Laukhin, S. I. Pesotskii, I. F. Schegolev, and V. M. Yakovenko, J. Phys. I **2**, 89 (1992).
[19] M. S. Nam, S. J. Blundell, A. Ardavan, J. A. Symington, and J. Singleton, J. Phys.: Condens. Matter **13**, 2271 (2001).

[20] P. D. Grigoriev, Phys. Rev. B **81**, 205122 (2010).
[21] A. J. Schofield and J. R. Cooper, Phys. Rev. B **62**, 10779 (2000).
[22] P. Moses and R. H. McKenzie, Phys. Rev. B **60**, 7998 (1999).
[23] Tsunea Ando, J. Phys. Soc. Jpn. **36**, 959 (1974).
[24] Tsunea Ando, J. Phys. Soc. Jpn. **36**, 1521 (1974).
[25] P. D. Grigoriev, M. V. Kartsovnik, W. Biberacher, and P. Wyder, arXiv:cond-mat/0108352; P. D. Grigoriev, Ph.D. thesis, University of Konstanz, 2002.
[26] T. Champel and V. P. Mineev, Phys. Rev. B **66**, 195111 (2002).
[27] P. D. Grigoriev, Phys. Rev. B **67**, 144401 (2003).
[28] V. M. Gvozdikov, Phys. Rev. B **70**, 085113 (2004).
[29] P. D. Grigoriev, Phys. Rev. B **83**, 245129 (2011).
[30] P. D. Grigoriev, JETP Lett. **94**, 47 (2011).
[31] P. D. Grigoriev, Low Temp. Phys. **37**, 738 (2011) [Fiz. Nizk. Temp. **37**, 930 (2011)].
[32] P. D. Grigoriev, Phys. Rev. B **88**, 054415 (2013).
[33] P. D. Grigoriev, M. V. Kartsovnik, and W. Biberacher, Phys. Rev. B **86**, 165125 (2012).
[34] D. Shoenberg, *Magnetic Oscillations in Metals* (Cambridge University Press, Cambridge, 1984).
[35] A. A. Abrikosov, *Fundamentals of the Theory of Metals* (North-Holland, Amsterdam, 1988).
[36] J. M. Ziman, *Principles of the Theory of Solids* (Cambridge University Press, Cambridge, 1972).
[37] A. D. Grigoriev and P. D. Grigoriev, Low Temp. Phys. **40**, 367 (2014) [Fiz. Nizk. Temp. **40**, 472 (2014)].
[38] Tsunea Ando, J. Phys. Soc. Jpn. **37**, 622 (1974).
[39] E. Brezin, D. I. Gross, and C. Itzykson, Nucl. Phys. B **235**, 24 (1984).
[40] M. E. Raikh and T. V. Shahbazyan, Phys. Rev. B **47**, 1522 (1993).
[41] A. M. Dyugaev, P. D. Grigor'ev, Yu. N. Ovchinnikov, JETP Lett. **78**, 148 (2003).
[42] I. S. Burmistrov and M. A. Skvortsov, JETP Lett. **78**, 156 (2003).
[43] K. B. Efetov and V. G. Marikhin, Phys. Rev. B **40**, 12126 (1989).
[44] I. V. Kukushkin, S. V. Meshkov, and V. B. Timofeev, Sov. Phys. Usp. **31**, 511 (1988).
[45] A. D. Mirlin, E. Altshuler, and P. Wölfle, Ann. Phys. (Leipzig) **5**, 281 (1996).
[46] I. A. Dmitriev, A. D. Mirlin, D. G. Polyakov, and M. A. Zudov, Rev. Mod. Phys. **84**, 1709 (2012).
[47] M. V. Kartsovnik, P. D. Grigoriev, W. Biberacher, and N. D. Kushch, Phys. Rev. B **79**, 165120 (2009).
[48] D. B. Gutman and D. L. Maslov, Phys. Rev. Lett. **99**, 196602 (2007); Phys. Rev. B **77**, 035115 (2008).
[49] A. A. Abrikosov, Physica C **317-318**, 154 (1999).
[50] Urban Lundin and Ross H. McKenzie, Phys. Rev. B **68**, 081101(R) (2003).
[51] A. F. Ho and A. J. Schofield, Phys. Rev. B **71**, 045101 (2005).
[52] *Spin Current*, Semiconductor Science and Technology, edited by Sadamichi Maekawa, Sergio O. Valenzuela, Eiji Saitoh, and Takashi Kimura (Oxford University Press, 2012).
[53] Igor Žutić, Jaroslav Fabian, and S. Das Sarma, Rev. Mod. Phys. **76**, 323 (2004).
[54] M. V. Kartsovnik, D. Andres, S. V. Simonov, W. Biberacher, I. Sheikin, N. D. Kushch, and H. Müller, Phys. Rev. Lett. **96**, 166601 (2006).